AIAA JOURNAL
Vol. 38, No. 2, February 2000

# Incidence Effects on Chordwise Bending Cascade Unsteady Aerodynamics

Daniel A. Ehrlich* and Sanford Fleeter†
*Purdue University, West Lafayette, Indiana 47907*

**Experiments directed at investigating and quantifying the effects of off-design conditions, including mean flow incidence and leading-edge flow separation, on chordwise bending mode unsteady aerodynamics are described. An influence coefficient technique is used wherein a single airfoil in the cascade is oscillated in a chordwise bending mode, accomplished with a piezoelectric crystal-based drive system. The resulting unsteady surface pressures on the oscillating airfoil and its stationary neighbors are measured and the unsteady aerodynamic influence coefficients determined, with the cascade unsteady aerodynamics defined through a vector summation. Unsteady aerodynamic data are obtained over a range of reduced frequency values and mean flow incidence angles, with the effects of steady loading and leading-edge separation examined. Significant effects of mean incidence on cascade unsteady aerodynamics that deviate significantly from linearized theory occur near the leading edge, with the nonlinear region increasing with increasing mean incidence. The large-scale effects of mean incidence on the leading-edge unsteady aerodynamic loading are attributable to both steady loading and suction surface separation.**

## Nomenclature

$A_c$ = chordwise bending mode shape amplitude
$C$ = airfoil chord
$C_p$ = unsteady surface pressure coefficient
$\hat{C}_p^n$ = unsteady pressure influence coefficient induced by airfoil $n$ oscillations
$h(x)$ = first harmonic normalized airfoil deflection
$k$ = reduced frequency, $(\omega C/U)$
$p_j$ = $j$th harmonic complex airfoil surface static pressure
$U$ = freestream velocity
$W_c$ = unsteady aerodynamic work per cycle
$\bar{W}_c$ = dimensionless unsteady aerodynamic work per cycle
$w$ = airfoil surface upwash velocity
$\bar{w}$ = complex amplitude of airfoil surface upwash velocity
$\bar{w}_c$ = pressure difference displacement function
$x$ = dimensionless airfoil chordwise coordinate or percent chord
$y$ = dimensionless coordinate normal to chordwise direction, $(Y/A_c)$
$\bar{y}$ = amplitude of airfoil surface displacement normal to chord
$\beta$ = cascade interblade phase angle (positive-airfoil $n+1$ leads airfoil $n$)
$\Delta C_L$ = coefficient of unsteady blade lift
$\Delta C_p$ = unsteady pressure difference coefficient
$\Delta \hat{C}_p^n$ = unsteady pressure difference influence coefficient
$\Delta L$ = unsteady airfoil lift
$\phi_p$ = unsteady pressure phase
$\omega$ = airfoil oscillation frequency

*Subscripts and Superscripts*

$j$ = $j$th harmonic of airfoil oscillation frequency
$p$ = airfoil pressure surface
$s$ = airfoil suction surface

## Introduction

RECENT efforts to increase gas turbine performance and reduce size and weight have led to changes in blade row design trends. Advanced turbomachinery feature closely spaced blade rows that utilize thin, low-aspect-ratio blading operating with high steady loading. Also, the mechanical damping is considerably reduced, particularly with integral blade–disk configurations (blisks) and in those without shrouds. As a result, these configurations are subject to higher stresses, both at and off-design, with low-aspect-ratio blading exhibiting significant unsteady flow-induced vibration problems. With the mechanical damping considerably reduced, the motion-induced unsteady aerodynamics or aerodynamic damping of the blade row determines the level of vibratory response. Thus, it is important to investigate and quantify the aerodynamic damping of low aspect ratio blade rows, particularly the effects of off-design conditions, including mean flow incidence and leading-edge flow separation.

The vibration characteristics of low aspect ratio blades more closely resemble plates than beams. They have chordwise bending natural frequencies within the engine operating range, resulting in flow-induced chordwise bending vibrations becoming a significant development problem. Low-aspect-ratio blade vibration frequencies, including chordwise bending modes, can be accurately predicted with finite element analyses. However, the emphasis of unsteady aerodynamics has been on the aerodynamic damping of vibration modes of importance to high-aspect-ratio blading, simple bending and torsion. To this end, a number of fundamental bending and torsion oscillating airfoil cascade experiments have been performed. Unfortunately, there is a dearth of fundamental unsteady aerodynamic data for the chordwise bending or two-stripe vibration modes exhibited by advanced low-aspect-ratio blading.

The chordwise bending unsteady aerodynamics of a subsonic flat plate airfoil cascade in a subsonic flow was studied experimentally by Ehrlich and Fleeter.[1] With zero mean flow incidence, these experiments simulated design point operating conditions. However, turbomachinery blade rows operate over a wide range of conditions, with off-design, nonzero mean incidence flow-induced vibrations being of significant concern. Mean flow incidence is a metric for the level of steady loading. Thus, it is well known to have significant effects on blade row steady aerodynamics, for example, flow separation, as well as unsteady aerodynamic response.

This paper describes a series of experiments directed at investigating and quantifying the effects of off-design conditions, including mean flow incidence and suction surface leading-edge region flow separation, on chordwise bending mode unsteady aerodynamics. An influence coefficient technique is used wherein a single airfoil in the cascade is oscillated in a chordwise bending mode, accomplished with a piezoelectric crystal-based drive system. The resulting unsteady pressures on the oscillating airfoil and its stationary neighbors are measured, and the unsteady aerodynamic influence coefficients determined, with the cascade unsteady aerodynamics

Received 16 July 1998; revision received 22 July 1999; accepted for publication 28 July 1999. 

*Cummins Fellow, School of Mechanical Engineering.
†McAllister Distinguished Professor, School of Mechanical Engineering.

defined through a vector summation. Unsteady aerodynamic data are obtained over a range of reduced frequency values and mean incidence angles, with the effects of steady loading and leading-edge separation examined.

## Influence Coefficient Technique

Oscillating airfoil cascade unsteady aerodynamic data are traditionally obtained by simultaneously oscillating all of the cascade airfoils at a constant interblade phase angle, with the unsteady airfoil surface pressures then measured. These experiments are extremely expensive, requiring complex drive systems to oscillate an entire cascade at realistic reduced frequencies and constant interblade phase angle. They are also time consuming because they must be performed over the complete interblade phase angle range.

The unsteady aerodynamic influence coefficient technique provides an alternative method for obtaining experimental oscillating cascade data. A single airfoil in the cascade is oscillated with the resulting unsteady pressure induced on this oscillating airfoil, and its stationary neighbors are measured. These unsteady pressures, expressed as pressure coefficients $\hat{C}_p^n(x)$, are the unsteady aerodynamic influence coefficients. The unsteady aerodynamics of a cascade having all airfoils oscillating at a specified constant interblade phase angle are then obtained through a vector summation of these unsteady aerodynamic influence coefficients.

Consider a two-dimensional flat plate airfoil cascade (Fig. 1) oscillating simultaneously with a constant interblade phase angle $\beta$. The unsteady pressure coefficient $C_p(x, \beta)$ on the surface of a reference airfoil, airfoil 0, is represented by a Fourier series summation of complex-valued unsteady aerodynamic influence coefficients:

$$C_p(x, \beta) = \sum_{n=-\infty}^{+\infty} \hat{C}_p^n(x) e^{in\beta} \tag{1}$$

where the index $n$ indicates that the influence coefficient $\hat{C}_p^n(x)$ represents the unsteady pressure coefficient induced on the reference airfoil by the oscillation of airfoil $n$.

For a specific cascade configuration, the unsteady aerodynamic influence coefficients $\hat{C}_p^n(x)$ can be determined from the unsteady surface pressure distribution on a typical airfoil in the cascade by inverting Eq. (1). In this manner, airfoil unsteady aerodynamics predicted by analytical oscillating cascade models can be used to calculate influence coefficients for comparison with data:

$$\hat{C}_p^n(x) = \frac{1}{2\pi} \int_{-\pi}^{\pi} C_p(x, \beta) e^{-in\beta} \, d\beta \tag{2}$$

Validation of the unsteady aerodynamic influence coefficient technique has been achieved by several researchers through comparison of influence coefficient results with data obtained from cascade experiments with all airfoils oscillating. Most recently, Kovats[2]

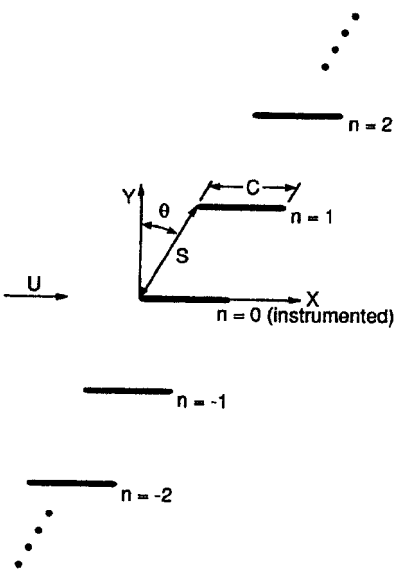


**Fig. 1 Two-dimensional infinite cascade model.**

showed favorable results for the comparison of predictions of aerodynamic damping and stability of low-pressure turbine blades. Buffum and Fleeter[3] also found good agreement between the influence coefficient method and all of the airfoils' oscillating data for torsion flutter in a linear cascade at moderate subsonic Mach numbers. The water channel results of Hanamura et al.[4] also appear to validate the unsteady aerodynamic influence coefficient technique.

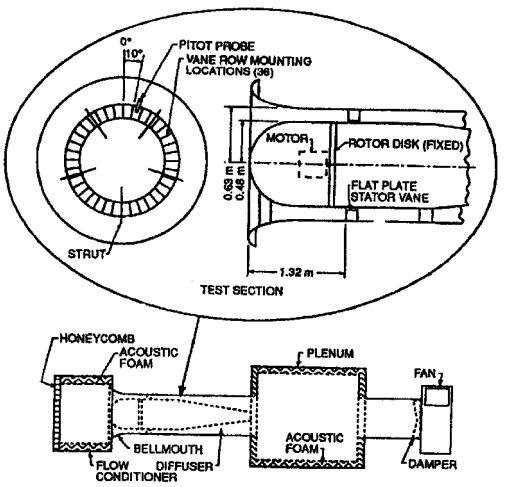


**Fig. 2 Purdue annular cascade research facility.**

## Experimental Facility

The chordwise bending experiments are conducted in the Purdue University annular cascade research facility (Fig. 2). It is an open-loop, draw through wind tunnel. A centrifugal fan downstream of the test section and driven by a 224-kW (300-hp) induction motor draws air through the facility. This fan is capable of producing steady test section velocities ranging from 6.4 m/s (20 ft/s) to 70 m/s (220 ft/s).

The test section is configured with an isolated row of 36 flat plate airfoils mounted at stagger angles of 0, 4, and 12 deg, thereby varying the steady loading and mean flow incidence. The airfoils have a chord length of 17.78 cm (7.0 in.) and a span of 14.99 cm (5.9 in.), resulting in an aspect ratio of 0.85 and a cascade solidity of 1.83. Of the 36, 34 airfoils are uninstrumented, having a thickness of 0.48 cm (0.1875 in.). A stationary airfoil is instrumented at midspan with a chordwise distribution of nine dynamic pressure transducers. To mount these transducers within the airfoil, its thickness is increased to 0.96 cm (0.375 in.). The final airfoil is the chordwise bending mode oscillating airfoil that is also instrumented at nine chordwise locations. Because an unsteady aerodynamic influence coefficient technique is used with one airfoil at a time oscillating, the different thickness airfoils should have only minimal, if any, effect on the resulting cascade data.

## Data Acquisition and Analysis

### Chordwise Bending Airfoil Oscillation

The unsteady surface pressure influence coefficient distributions are produced by the two-dimensional chordwise bending mode oscillation of a single flat plate airfoil constructed from a 0.038-cm-(0.015-in.-) thick sheet of stainless steel. The oscillating airfoil and mounting configuration (Fig. 3) are designed to maximize the amplitude and two dimensionality of the chordwise bending mode. It is designed to resonate in a two-dimensional chordwise bending mode at a frequency of 66 Hz when excited by a set of four surface bonded piezoceramic motor elements.[1]

Oscillating airfoil motion is determined by measurement of the airfoil mounting shaft's rotational oscillation. The oscillating airfoil leading- and trailing-edge shafts are affixed with linear taper precision potentiometers. Output of front and rear airfoil shaft potentiometer circuits are calibrated against airfoil leading- and trailing-edge midspan surface deflection measurements made using an Omron model 3Z4M laser displacement sensor. Shaft potentiometer circuit calibrations are performed in a calibration wind tunnel at freestream velocities of 38.5, 25.5, and 19.1 m/s (121, 80.6,

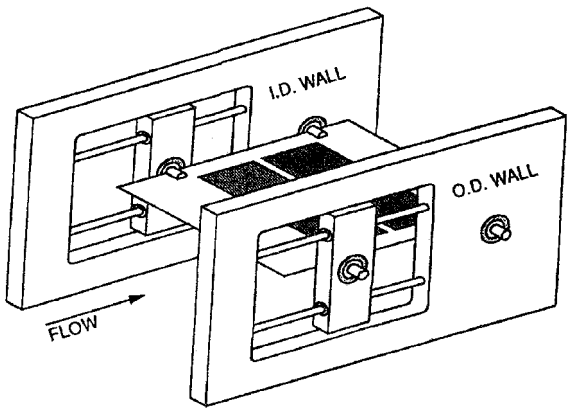


**Fig. 3 Chordwise bending oscillating airfoil mounting configuration.**

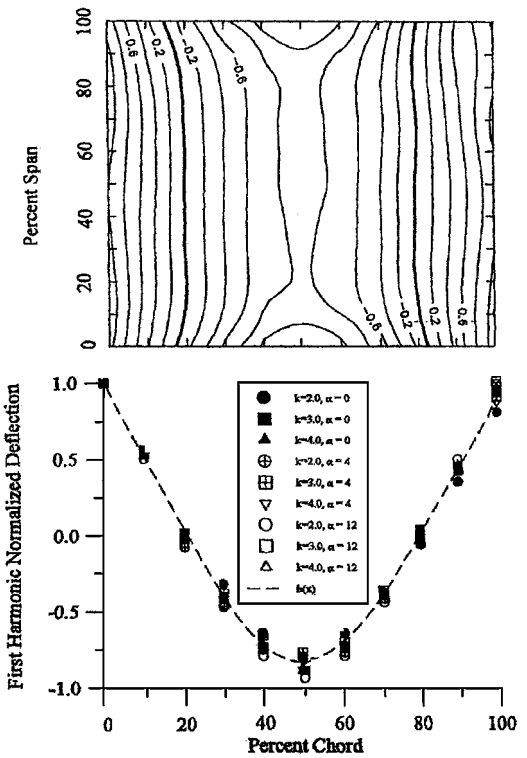


**Fig. 4 Oscillating airfoil mode shape.**

and 60.5 ft/s), corresponding to reduced frequencies of $k = 2$, 3, and 4.

The oscillating airfoil mode shape is determined by measuring the airfoil surface displacement at points on a $5 \times 11$ point rectangular grid with surface displacement data acquired at a sampling rate of 1000 Hz in 2-s bursts. The airfoil surface displacement time traces are Fourier transformed to obtain displacement magnitude and phase information at each grid point. Airfoil motion is primarily contained within the first harmonic, with higher harmonic magnitudes always being less than 10% of the first harmonic. First harmonic phase information determines the mode-shape node line locations. The chordwise bending mode shape is characterized by the normalized first harmonic midspan cross section of the airfoil surface displacement $h(x)$ with the periodic airfoil motion described by

$$Y(x, t) = Re\left[A_c h(x) e^{i\omega t}\right] \tag{3}$$

where $A_c$ is the midspan leading-edge surface displacement, with the positive leading edge up.

Figure 4 presents normalized first harmonic mode-shape data for the chordwise bending airfoil. The nearly straight chordal contour lines indicate that the airfoil oscillates in a two-dimensional mode. The mode exhibits two chordal node lines at the airfoil shaft locations of 20 and 80% chord, identified as bold contours. The midspan cross-sectional mode data show a very slight dependence on reduced frequency and incidence. However, the airfoil is able to be characterized by a single normalized mode-shape curve $h(x)$ obtained by fitting the nine mode shape data sets with a sixth-order polynomial using the least-squares method.

### Unsteady Airfoil Surface Pressures

The magnitude and phase of the unsteady airfoil surface pressures induced by the chordwise bending oscillation of a single airfoil in the annular airfoil cascade are measured using PCB Piezotronics Model 103A piezoelectric dynamic pressure transducers. Transducer signals are amplified to required levels using a 12-channel instrumentation amplifier and power supply.

Unsteady pressure measurements are made on both the stationary airfoil and the chordwise bending oscillating airfoil at nine chordwise locations, 2.5, 10.7, 23.2, 35.7, 50.0, 64.3, 76.5, 89.3, and 97.5% chord. On the stationary airfoil, nine PCB dynamic pressure transducers are mounted inside the rigid airfoil. For the chordwise bending oscillating airfoil, the elastic airfoil deformation restricts the method in which surface pressure measurements can be made. Thus, the nine PCB dynamic pressure transducers are mounted external to the chordwise bending oscillating airfoil and connected to midspan static pressure taps by sensing lines. This transducer configuration is chosen because the mass of the transducers mounted on the airfoil surface would represent a significant percentage of the airfoil mass and would distort the chordwise bending mode shape. Mounting the transducers in the stationary frame also eliminates problems associated with subjecting the transducers to plate surface accelerations to $32g$. Dynamic pressure sensing line systems exhibit nonlinear response and must, therefore, be calibrated to correct for passage effects. Hoyniak and Fleeter[5] have shown that dynamic pressure transducer sensing lines can be calibrated for the accurate measurement of unsteady pressures having frequencies that are well below the natural frequency of the sensing system. Dynamic calibration of the chordwise bending oscillating airfoil pressure sensing lines is performed in a resonator tube in a manner similar to that used by Henderson and Fleeter.[6] Calibration of the oscillating airfoil pressure sensing lines shows that the frequency of interest, 66 Hz, is well below the natural frequency of the sensing system that is approximately 350 Hz. Unsteady pressures having a fundamental frequency of 66 Hz can, therefore, be accurately measured through the transducer sensing line systems.

### Unsteady Aerodynamic Influence Coefficients and Airfoil Loading

Cascade chordwise bending unsteady aerodynamic loading is determined by the influence coefficient technique. With the oscillating airfoil driven in the chordwise bending mode at 66 Hz, the unsteady surface pressures induced by the oscillating airfoil on itself and its stationary neighbors are measured at freestream velocities corresponding to reduced frequencies of $k = 2$, 3, and 4 at mean incidence angles of 0, 4, and 12 deg. First, the oscillating airfoil data determine the self-induced unsteady aerodynamics. Data from the leading- and trailing-edge airfoil shaft potentiometer circuits and the pressure transducers are acquired at a sampling rate of 5000 Hz. From each transducer, 100 bursts of 5000 samples of data representing 66 chordwise bending airfoil oscillation cycles are acquired.

Next, the unsteady pressures on the stationary airfoils generated by the oscillating airfoil are measured. Unsteady pressure and suction surface pressure data are obtained with the oscillating airfoil in relative positions $n = -1$ and 1 (Fig. 1). Unsteady surface pressures on the reference airfoil with the oscillating airfoil in positions where $|n| \leq 1$ were found to comprise 94% of the unsteady loading and influence coefficients induced by the oscillating airfoil in positions with $|n| > 1$ are, therefore, neglected.[1]

The 100 bursts of airfoil surface pressure data acquired at each transducer location are ensemble averaged to eliminate pressure fluctuations not phase locked to the oscillating airfoil motion. The resulting representative unsteady pressure signal is then Fourier transformed to obtain unsteady airfoil surface pressure magnitude and phase information. The chosen acquisition sampling rate and duration provide a 1.0-Hz Fourier transform frequency resolution. Harmonic pressure signal magnitudes and phases for frequencies

corresponding to the first four harmonics of the airfoil oscillation frequency, 66, 132, 198, and 264 Hz, are extracted from the transformed signals and adjusted to account for the effects of the transducer mounting passages on the frequency response, as determined from dynamic calibrations. In all cases, airfoil surface pressure response is negligible at frequencies not corresponding to blade motion harmonics. Airfoil motion magnitude and phase are determined by averaging, transforming, and scaling the oscillating airfoil leading-edge potentiometer circuit signal in a manner similar to that for the pressure signals. The airfoil motion is harmonic with motion at the driving frequency of 66 Hz accounting for greater than 90% of the airfoil motion and higher harmonic motion, if present, appearing in the second harmonic of the airfoil driving frequency. Airfoil motion at other frequencies is negligible. Airfoil surface pressures are referenced to the airfoil motion.

The complex-valued unsteady aerodynamic pressure and pressure difference influence coefficients are defined as

$$\hat{C}_p^n(x) = \frac{p_1(x)}{\rho_0 U^2 (A_c/C)}, \qquad \Delta\hat{C}_p^n = \hat{C}_{pu}^n - \hat{C}_{pl}^n \tag{4}$$

where $p_1(x)$ is the complex surface static pressure corresponding to the $j$th harmonic of the airfoil oscillation frequency and the subscripts $u$ and $l$ indicate upper and lower airfoil surfaces.

The unsteady aerodynamics of a cascade having all airfoils oscillating at specified interblade phase angles are determined through a vector summation of the unsteady aerodynamic influence coefficients per Eq. (1), with summation limits from $n = -1$ to 1.

## Results and Discussion

The chordwise bending unsteady aerodynamics of an annular cascade of flat plate airfoils are experimentally investigated, with data obtained at mean flow incidence angles of 0, 4, and 12 deg over a range of reduced frequency values. An unsteady aerodynamic influence coefficient technique is utilized, with the influence coefficient data summed vectorially to determine the airfoil unsteady surface pressure distributions for a cascade having all airfoils oscillating at interblade phase angles of $\beta = 0$, 90, and 180 deg.

As a reference, data are correlated with predictions from LINSUB,[7] which solves the inviscid subsonic linearized continuity and momentum equations for a two-dimensional cascade of zero mean incidence oscillating flat plate airfoils. To predict chordwise bending mode unsteady aerodynamics, the LINSUB boundary conditions are modified. The airfoil surface flow tangency boundary condition is enforced by equating the normal flow velocity on the airfoil surface to the velocity of the moving airfoil surface. The nondimensional velocity normal to the airfoil surface, the upwash, for an arbitrary harmonic airfoil motion $y = \bar{y}(x)e^{i\omega t}$ is

$$\frac{\bar{w}(x)}{U} = \frac{\partial \bar{y}(x)}{\partial x} + ik\bar{y}(x) \tag{5}$$

where $\bar{y}(x)$ and $\bar{w}(x)$ are the airfoil oscillation and upwash oscillation amplitude distributions.

Chordwise bending mode oscillations are specified by the airfoil oscillation amplitude:

$$\bar{y}(x) = (A_c/C)h(x) \tag{6}$$

where $A_c$ and $h(x)$ are the measured chordwise bending amplitude and normalized mode shape.

### Airfoil Steady Loading and Separation Characteristics

Three mean incidence angles are considered: 0, 4, and 12 deg. The $\alpha = 0$ deg data serve as a baseline, having no steady loading and matching the LINSUB modeling. At 4 and 12 deg mean incidence, the airfoils have steady loading and, as determined by steady flow visualization experiments, exhibit a leading-edge separation bubble. At steady freestream velocities corresponding to $k = 2$, 3, and 4, the chordwise extent of the separation bubbles increase with increasing mean flow incidence and decrease with increasing steady velocity (Table 1).

**Table 1 Steady leading-edge separation bubble length (% chord)**

| | $U$, ft/s | | |
|---|---|---|---|
| $\alpha$, deg | 60.5 | 80.6 | 121 |
| 4 | 10 | 9 | 8 |
| 12 | 35 | 31 | 27 |

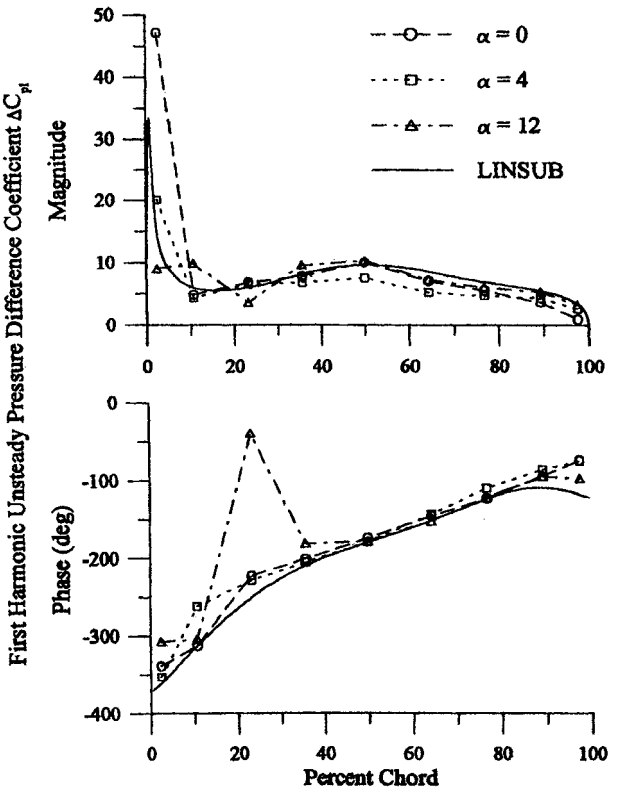


**Fig. 5 First harmonic unsteady pressure difference coefficient distribution: $k = 2.0$ and $\beta = 0$ deg.**

### Chordwise Bending Unsteady Aerodynamics

Representative chordwise bending unsteady pressure distributions are determined from the measured unsteady pressure influence coefficients for interblade phase angles of $\beta = 0$, 90, and 180 deg. The 99% confidence uncertainties are ±8% in magnitude and ±6 deg in phase.

The cascade unsteady aerodynamics are obtained with the chordwise bending airfoil oscillating harmonically at 66 Hz with a leading-edge deflection amplitude of ±1.0% chord corresponding to a change from −3 to ± 3 deg in instantaneous leading-edge flow incidence angle. For a linear system, response is expected exclusively at the frequency of motion of the oscillating airfoil. A nonlinear system, however, will evoke response at frequencies other than the frequency at which it is excited. For the chordwise bending cascade studied herein, the airfoil motion amplitude is small and limited primarily to a single frequency. Under these conditions, the system is expected to exhibit linear response characteristics. However, leading-edge separation, if present, may introduce nonlinearities producing response at harmonics of the airfoil motion frequency because the separation is a result of this motion. To this end, the linear system response at the airfoil oscillation frequency is first considered. Nonlinear system response, that is, response at higher harmonics, is then examined.

Figures 5–7 present the first harmonic unsteady pressure difference coefficients at mean incidence angles of 0, 4, and 12 deg and the linear theory prediction at $k = 2$, 3, and 4 and $\beta = 0$ deg. This corresponds to a superresonant cascade mode, with waves propagating away from the oscillating airfoil row unattenuated. Two phenomena affect the unsteady aerodynamic loading of a cascade at positive mean incidence: steady loading and the formation of a leading-edge separation bubble. Both effects are evident in the data.

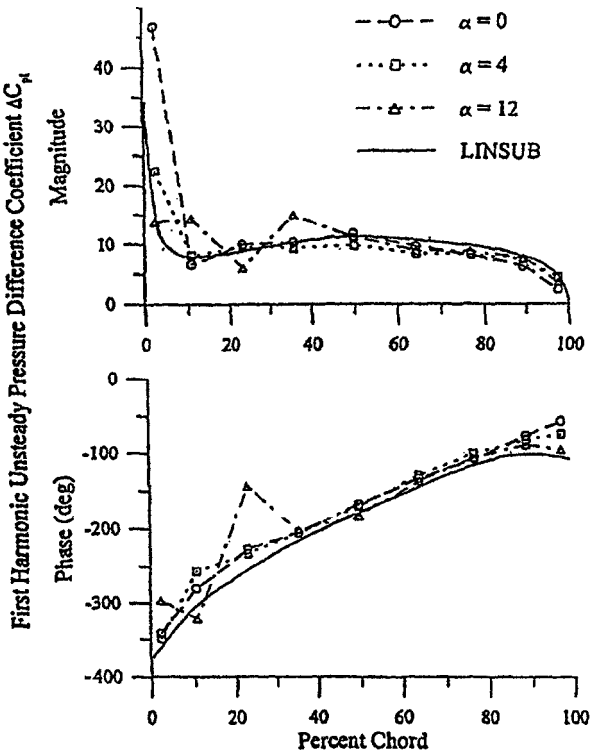


**Fig. 6 First harmonic unsteady pressure difference coefficient distribution: $k = 3.0$ and $\beta = 0$ deg.**

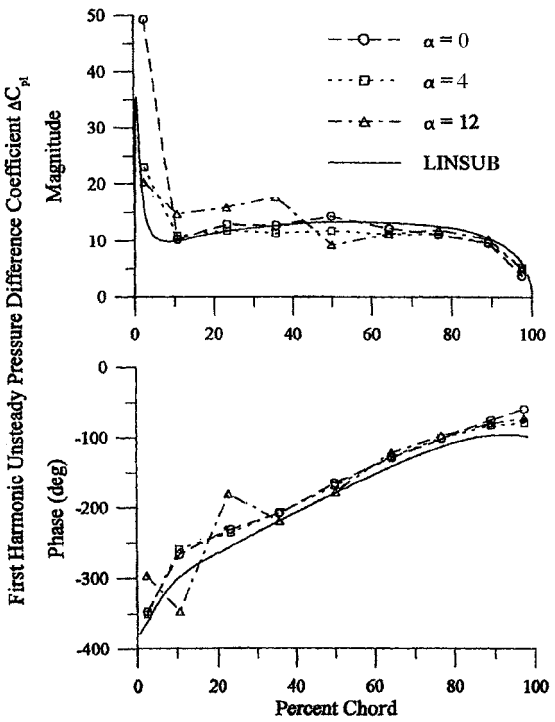


**Fig. 7 First harmonic unsteady pressure difference coefficient distribution: $k = 4.0$ and $\beta = 0$ deg.**

Figure 5 shows the effect of steady loading and mean incidence on the airfoil surface pressure difference data at $k = 2$ and $\beta = 0$ deg. The $\alpha = 0$ deg magnitude data attain a maximum near the leading edge, rapidly decrease to a local minimum near 10% chord, then increase to a local maximum near 50% chord, and decrease to near zero at the trailing edge. The chordwise unsteady pressure difference phase distribution is nearly linear with chord, out of phase with the airfoil motion at the leading edge, lagging the airfoil motion over the forward half of the airfoil while leading the motion over the aft half of the airfoil.

As the mean incidence is increased, there is a considerable reduction in the first harmonic magnitude in the leading-edge region. This is attributed to the leading-edge suction surface separation bubble, with steady separation experiments having shown an 9%-chord-long bubble at 4-deg incidence and a 31%-chord-long bubble at $\alpha = 12$ deg. The chordwise extent of these steady flow separation bubbles is indicative of the size of the separated regions during small-amplitude chordwise bending oscillation. The differences between the unsteady aerodynamics at $\alpha = 0$ and 4 deg aft of 20% chord are attributed primarily to steady loading effects, whereas the unsteady loading distribution at $\alpha = 12$ deg is due to the combined effect of steady loading and the formation of a large leading-edge separation bubble. In the midchord region between the chordwise bending node lines at 20 and 80% chord, the $\alpha = 4$ deg data show slightly decreased unsteady loading as compared to the baseline. However, the $\alpha = 12$ deg data show the loading magnitude is reduced just aft of 20% chord, exceeds the baseline loading at 35% chord, and is essentially equal to the baseline loading between 50 and 80% chord. With the exception of slight differences in and around the leading-edge separation bubble and the discontinuity near the $\alpha = 12$-deg separation bubble reattachment point, the unsteady pressure difference phase distribution data at $\alpha = 0$, 4, and 12 deg mean incidence are essentially identical. The linear predictions generally correlate well with the data, the exception being the leading-edge unsteady loading magnitude, attributed primarily to separation effects. Also, unpredicted discontinuities in phase are observed near the leading-edge separation bubble reattachment point.

The trends exhibited by the $k = 3$ and 4 data are similar to those seen at $k = 2$, with an increase in the unsteady loading magnitude over the entire airfoil surface (Figs. 6 and 7). However, leading-edge unsteady loading distortion at $\alpha = 12$ deg is more pronounced. This is due to the reduced frequency being increased by decreasing the freestream velocity, thereby resulting in a longer leading-edge separation bubble. Thus, the increases in unsteady pressure difference magnitude in the $k = 2$ data at 10 and 37% chord attributed to the leading-edge separation bubble motion are larger in the $k = 3$ data. Discontinuities in the unsteady pressure difference phase are again seen at the steady separation bubble reattachment points at both $\alpha = 4$ and 12 deg. As expected, the trends in the unsteady pressure difference magnitude and phase distributions remain unchanged whereas the magnitude of the unsteady loading over the entire airfoil surface increases with the increase in reduced frequency. Discontinuities in phase are still present near the steady flow reattachment points.

Further insight into the effects of steady loading and leading-edge separation on the unsteady aerodynamics of a chordwise bending cascade is gained by examining the airfoil pressure and suction surface unsteady pressure coefficients individually. Pressure and suction surface first harmonic unsteady pressure coefficient distributions for $\alpha = 0$, 4, and 12 deg and $\beta = 0$ deg at a $k = 3$ are presented in Figs. 8 and 9.

The pressure surface leading edge unsteady pressure magnitude decreases with increasing mean incidence, with a major decrease from $\alpha = 0$ to 4 deg and an additional minor decrease to $\alpha = 12$ deg. With the chordwise bending airfoil oscillations, the mean incidence at the leading edge changes over an oscillation cycle. The oscillation amplitude is such that the instantaneous incidence ranges from $-3$ to $+3$ deg at zero mean incidence. As the airfoil oscillates between positive and negative incidence, the pressure and suction surfaces reverse roles, with the pressure surface becoming the suction surface at negative instantaneous incidence. This results in the large pressure fluctuations near the leading edge. The 9%-chord steady separation bubble at $\alpha = 4$ deg suggests that at zero mean incidence, a dynamic separation bubble alternately forms and collapses on the pressure and suction surfaces. When the mean incidence is increased to 4 and 12 deg, the instantaneous incidence is positive through the entire airfoil motion, and the pressure surface is no longer prone to separation during the oscillation. This results in reduced pressure surface unsteady loading magnitude. Aft of 10% chord, the unsteady loading magnitude increases with increasing mean incidence, attributed to increased steady loading.

On the suction surface, increasing the mean incidence also decreases the leading-edge unsteady pressure magnitude but not as

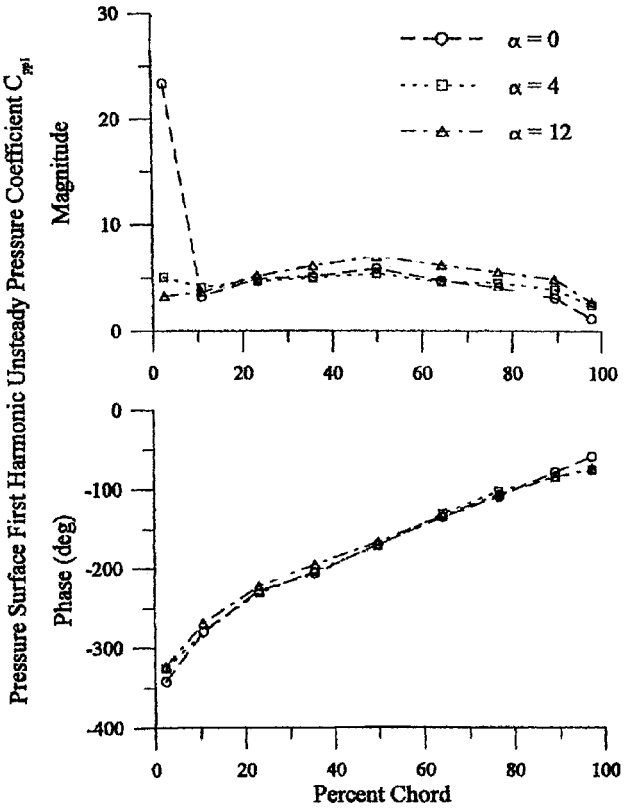


**Fig. 8 Pressure surface first harmonic unsteady pressure coefficient distribution: $k = 3.0$ and $\beta = 0$ deg.**

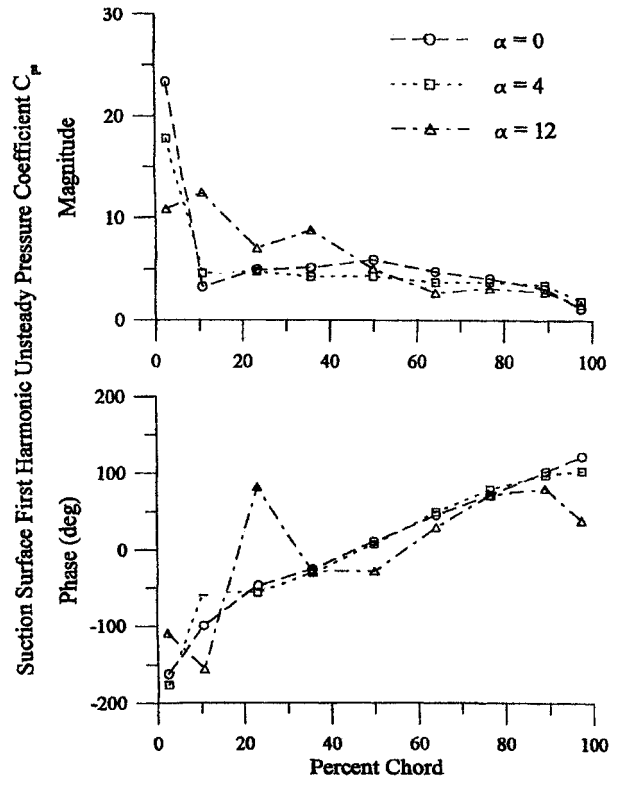


**Fig. 9 Suction surface first harmonic unsteady pressure coefficient distribution: $k = 3.0$ and $\beta = 0$ deg.**

pronounced as on the pressure surface. At zero mean incidence, flow symmetry dictates that pressure and suction surfaces exhibit the same response with a 180-deg phase shift, thus, the high suction surface leading-edge unsteady loading. The steady separation experiments suggest that increasing the mean incidence to 4 deg, the 9%-chord-long leading-edge separation bubble grows and remains present over a longer portion of the oscillation cycle, or no longer completely collapses but only changes length during an oscillation cycle, with this separation bubble damping the suction surface unsteady surface pressure. Aft of 10% chord with $\alpha = 4$ deg, the separation bubble no longer affects the unsteady pressure magnitude, and the reduction seen in the unsteady pressure magnitude distribution is attributed to steady loading. At $\alpha = 12$ deg, the steady separation bubble extends to approximately 37% chord, resulting in the increase in unsteady loading magnitude between 10 and 37% chord. Between 37 and 65% chord, the unsteady pressure magnitude falls off rapidly due to a combination of separation and steady loading effects. Discontinuities in the unsteady pressure phase that are absent from the pressure surface data appear near the steady separation bubble reattachment points, supporting the hypothesis that these discontinuities are the result of separation.

Figures 10 and 11 show the first harmonic unsteady pressure difference data at $k = 3$ and $\beta = 90$ and 180 deg. These cascades are subresonant, that is, waves decay exponentially with distance from the oscillating airfoil row. The trends in the unsteady pressure difference magnitude and phase data follow those of the superresonant case. The unsteady pressure magnitudes increase with increasing interblade phase angle over the entire airfoil surface. Agreement between these subresonant data and linear theory is not as satisfactory as in the superresonant case. The unsteady pressure difference magnitudes aft of 10% chord are overpredicted in all cases, with this overprediction increasing with interblade phase angle. As in the superresonant case, the leading-edge region unsteady pressure difference magnitudes are significantly underpredicted at $\alpha = 0$ deg, with predictions improving with increasing mean incidence.

The nonlinear unsteady aerodynamic response at higher harmonics of the oscillation frequency is now examined. The chordwise bending oscillating airfoil resonant drive system is designed to provide purely harmonic motion at a discrete frequency. However, small amplitude higher harmonics of the forcing frequency are present in the airfoil motion. The magnitudes of these higher harmonic motions are less than 1% of the fundamental airfoil motion magnitude at all frequencies and mean incidence angles with the exception of the second harmonics at $\alpha = 4$ and 12 deg, which are 4 and 9%, respectively. Thus, any airfoil loading response at frequencies other than the fundamental are attributed to nonlinear system response.

Figures 12–14 show first, second, third, and fourth harmonic ($n = 1, 2, 3, 4$) airfoil pressure and suction surface unsteady pressure

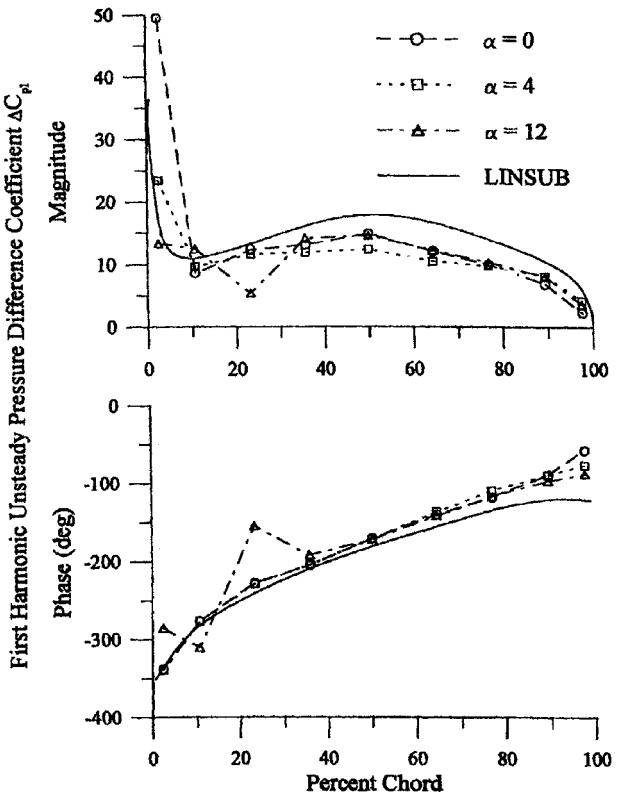


**Fig. 10 First harmonic unsteady pressure difference coefficient distribution: $k = 3.0$ and $\beta = 90$ deg.**

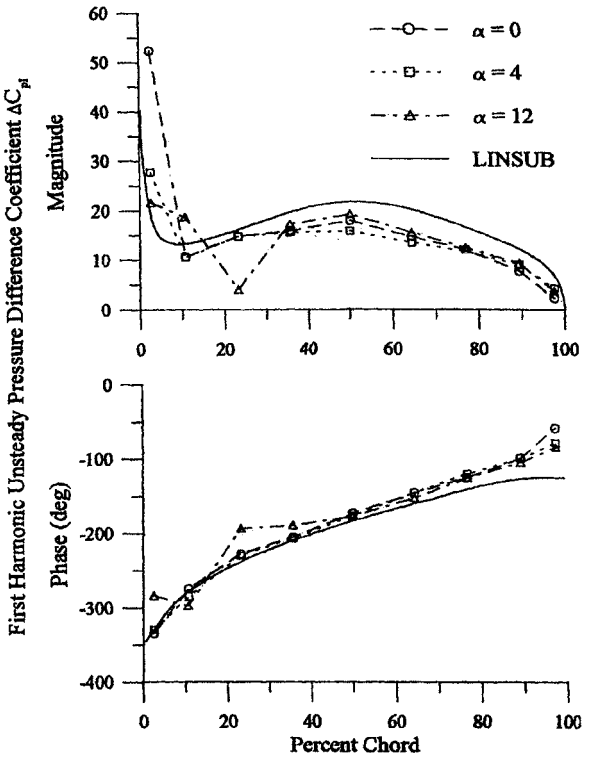


**Fig. 11 First harmonic unsteady pressure difference coefficient distribution: $k = 3.0$ and $\beta = 180$ deg.**

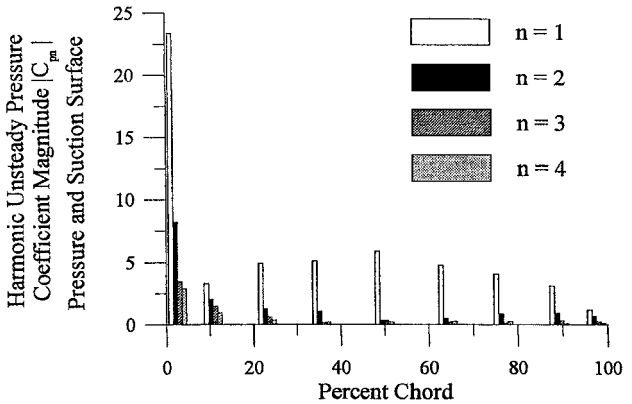


**Fig. 12 Harmonic unsteady pressure coefficient magnitude distribution: $\alpha = 0$ deg, $k = 3.0$, and $\beta = 0$ deg.**

coefficient magnitudes at $k = 3$ and $\beta = 0$ deg at mean incidence angles of 0, 4, and 12 deg.

At $\alpha = 0$ deg, significantly higher harmonic loadings are present on both the pressure and suction surfaces near the leading and trailing edges, with minimally higher harmonic response near midchord. The largest higher harmonic loading is seen near the airfoil leading edge, where the formation of a dynamic leading-edge separation bubble is expected. Additional higher harmonic activity is seen near the trailing edge and may be due to trailing-edge separation.

Increasing $\alpha$ to 4 deg results in suction surface loadings that are similar to those for $\alpha = 0$ deg, with magnitudes at all harmonics reduced over the entire chord. Again, leading-edge higher harmonic loadings are highest due to the separated flow. As expected, there is minimally higher harmonic response on the pressure surface where dynamic separation has been eliminated at positive incidence.

Further increasing the steady loading to $\alpha = 12$ deg, the suction surface higher harmonic loading magnitude data differ considerably from those at $\alpha = 0$ and 4 deg. Higher harmonic loadings at the airfoil leading edge are diminished whereas loadings between 10 and 40% chord increase considerably. At this high mean incidence, a steady separation bubble on the airfoil suction surface extends to 31%

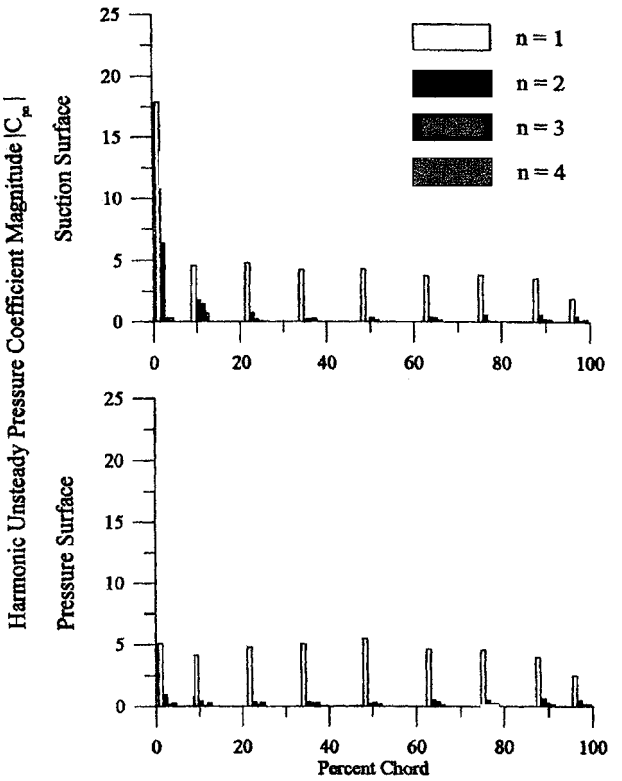


**Fig. 13 Harmonic unsteady pressure coefficient magnitude distribution: $\alpha = 4$ deg, $k = 3.0$, and $\beta = 0$ deg.**

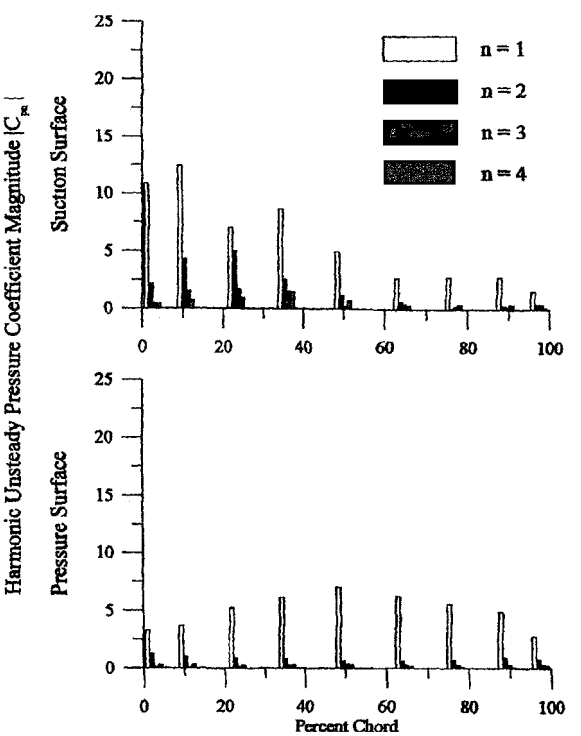


**Fig. 14 Harmonic unsteady pressure coefficient magnitude distribution: $\alpha = 12$ deg, $k = 3.0$, and $\beta = 0$ deg.**

chord. Dynamically, it is expected that this 31%-chord-long separation bubble advances and retreats along the suction surface in this region, introducing substantial higher harmonic loading. On the pressure surface, as at $\alpha = 4$ deg, minimally higher harmonic loadings are observed.

The unsteady lift coefficient provides an overall measure of the effect of cascade unsteady aerodynamics on the airfoil loading:

$$\Delta C_L = \Delta L / \rho_0 U^2 \tag{7}$$

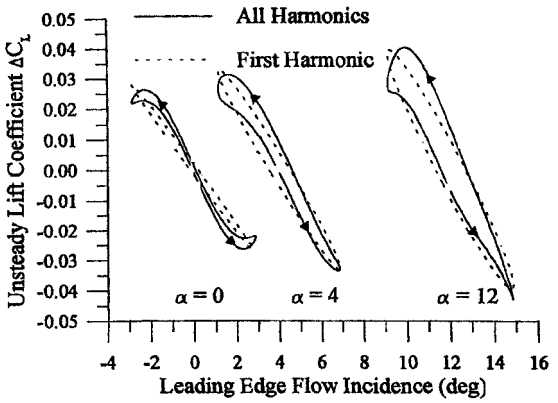


**Fig. 15 Unsteady lift coefficient through one oscillation cycle: $k = 3.0$ and $\beta = 0$ deg.**

where $\Delta L$ is the airfoil instantaneous lift minus the time mean lift, positive upward.

Figure 15 shows the instantaneous unsteady lift coefficient over one cycle of motion at $k = 3$, $\beta = 0$ deg, and mean incidence angles of 0, 4, and 12 deg. Both the measured lift and the lift due only to first harmonic unsteady loading are shown, with the lift loops traversed counterclockwise as time progresses. Mean incidence significantly affects the oscillating airfoil unsteady lift. As the mean incidence is increased, the envelope of unsteady lift increases, indicated by the increasing lift loop size. This demonstrates the coupling between steady loading and the unsteady aerodynamics. Note that, unlike an airfoil oscillating in torsion, lift decreases with increasing instantaneous leading-edge incidence and increases with decreasing instantaneous incidence. This suggests that the airfoil camber change due to the chordwise bending motion dominates the effect of increased leading-edge incidence. As the airfoil leading edge pitches up, the trailing edge pitches up an equal amount, thereby inducing negative camber in the instantaneous airfoil shape. Despite the positive incidence at the leading edge, negative lift is induced by the negative camber. As the airfoil leading edge pitches down, leading-edge incidence is reduced, but the airfoil motion produces positive camber that increases lift.

The shape of the lift loops also change with increasing mean incidence. At $\alpha = 0$ deg, symmetry exists between the positive and negative instantaneous incidence portions of the lift loop. This is due to the role reversal of the airfoil pressure and suction surfaces discussed earlier. The $\alpha = 0$ deg data also show a relatively smooth transition from increasing to decreasing lift and vice versa near the limits of blade travel. Increasing the mean incidence to 4 deg destroys the lift loop symmetry, as expected. The transition from increasing to decreasing lift as the airfoil moves through its minimum instantaneous incidence becomes smoother, whereas the transition from decreasing to increasing lift at maximum instantaneous incidence becomes more abrupt. This may be due to the suction surface leading-edge separation bubble forming and collapsing near maximum incidence and the lach of separation bubble near minimum incidence. Increasing $\alpha$ to 12 deg, this trend is further exaggerated, with an abrupt change from decreasing to increasing lift now present at maximum incidence. The change in character of the lift loops containing all harmonics of airfoil response is not seen in the elliptical first harmonic lift loops, thereby demonstrating the inability of a first harmonic analysis to capture nonlinear separation events.

## Conclusions

A series of experiments was performed directed at investigating and quantifying the effects of off-design conditions, including mean flow incidence and suction surface leading-edge region flow separation, on chordwise bending mode unsteady aerodynamics. An influence coefficient technique was used wherein a single airfoil in the cascade was forced to oscillate in a chordwise bending mode, accomplished with a piezoelectric crystal-based drive system. The resulting unsteady surface pressures on the oscillating airfoil and its stationary neighbors were measured, the unsteady aerodynamic influence coefficients determined, with the cascade unsteady aerodynamics defined through a vector summation. Unsteady aerodynamic data were obtained over a range of reduced frequency values and mean flow incidence angles, with the effects of steady loading and leading-edge separation examined. The first harmonic unsteady surface loadings were correlated with linear theory.

A peak in the first harmonic unsteady loading magnitude that diminishes with increasing mean incidence occurs near the leading edge. At both 4- and 12-deg mean incidence, a suction surface discontinuity in the phase of the first harmonic unsteady loading occurs near the leading-edge separation bubble reattachment position. Agreement between data and linear theory unsteady loading aft of 40% chord is good but exhibits dependence on the cascade mode, being better when the cascade is superresonant than when it is subresonant.

Higher harmonic loadings of significant amplitude are limited to the leading-edge region for 0- and 4-deg mean incidence, whereas significant higher harmonic loadings extend to nearly 40% chord at 12-deg mean incidence. Also, camber effects dominated the unsteady lift characteristics of the chordwise bending oscillating airfoil cascade.

At $\alpha = 0$ deg, a small leading-edge separation bubble persists for a portion of the airfoil chordwise bending motion. By the increase of the mean incidence to 4 deg, the separation bubble no longer appears on the airfoil pressure surface whereas the suction surface separation bubble grows slightly and/or persists for a longer portion of the oscillation cycle. At $\alpha = 12$ deg, the suction surface leading-edge separation bubble persists over the entire airfoil motion cycle and advances farther along the chord. The leading-edge separation bubble both introduces nonlinear higher harmonic response and distorts the first harmonic response to the chordwise bending oscillations. Also, increasing the mean incidence also increases the steady aerodynamic cascade loading.

## Acknowledgment

This research sponsored, in part, by the U.S. Army Research Office. This support is most gratefully acknowledged.

## References

[1] Ehrlich, D., and Fleeter, S., "Chordwise Bending Cascade Aerodynamics by an Experimental Influence Coefficient Technique," *Journal of Propulsion and Power*, Vol. 13, No. 1, 1997, pp. 39–48.

[2] Kovats, Z., "Predicting Aerodynamic Damping and Stability of Low Pressure Turbine Blades Using the Influence Coefficient Method," *ASME COGEN-TURBO International Gas Turbine Institute*, No. 6, 1991, pp. 251–262.

[3] Buffum, D. H., and Fleeter, S., "Aerodynamics of a Linear Oscillating Cascade," NASA TM 103250, Aug. 1990.

[4] Hanamura, Y., Tanaka, H., and Yamaguchi, K., "A Simplified Method to Measure Unsteady Forces Acting on the Vibrating Blades in Cascade," *Bulletin of the Japan Society of Mechanical Engineers*, Vol. 23, No. 180, 1980, pp. 880–887.

[5] Hoyniak, D., and Fleeter, S., "Frequency Response of Dynamic Pressure Transducer Sensing Line Configurations," *28th International Instrumentation Symposium*, Instrumentation Society of America, 1982.

[6] Henderson, G. H., and Fleeter, S., "Forcing Function Effects on Unsteady Aerodynamic Gust Response, Part II: Low Solidity Airfoil Row Response," *Journal of Turbomachinery*, Vol. 115, No. 4, 1993, pp. 751–761.

[7] Smith, S. N., "Discrete Frequency Sound Generation in Axial Flow Turbomachines," Aeronautical Research Council Repts. and Memoranda 3709, London, March 1972.

M. Samimy
*Associate Editor*